Available online at www.sciencedirect.com
ScienceDirect
Trans. Nonferrous Met. Soc. China 29(2019) 1365−1374
Transactions of Nonferrous Metals Society of China
www.tnmsc.cn

Influence of chemical modification by Y_2O_3 on eutectic Si characteristics and tensile properties of A356 alloy

M. E. MOUSSA[1], S. EL-HADAD[1], W. KHALIFA[2]

1. Department of Casting Technology Central Metallurgical Research and Development Institute (CMRDI), P. O. 87, Helwan, Egypt;
2. Department of Mining, Petroleum and Metallurgical Engineering, Faculty of Engineering, Cairo University, P. O. 12613, Giza, Egypt

Received 7 September 2018; accepted 27 February 2019

Abstract: The modification of A356 aluminum−silicon alloy using yttrium oxide (Y_2O_3) was studied. Addition levels of up to 2.5 wt.% Y_2O_3 were investigated. A premixed powder of Al−30wt.%Y_2O_3 was added to the melt at about 750 °C using vortex method. Samples were then poured in sand mold. The results showed that evident modification was obtained using the Y_2O_3 addition. The optimum level was 1.5 wt.%, and was corresponding to a eutectic temperature depression from 568 to 557 °C. The eutectic Si particles were refined in length from 44.8 to 8.3 μm, and modified in aspect ratio from 6.8 to 0.98. Higher additions of Y_2O_3 caused de-modification of the eutectic Si particles. The ductility of the modified specimens was enhanced by more than 20% compared to the unmodified ones. This was associated with a gradual transfer from cleavage to a more ductile mode of fracture.
Key words: hypoeutectic Al−Si alloys; modification; yttrium oxide (Y_2O_3); ductility; fracture mode

1 Introduction

The series of aluminum cast alloys based on the Al−Si system are the most frequently used Al-alloys group due to their combination of properties such as castability, specific strength and resistance to corrosive attack. Hypoeutectic Al−Si alloys specifically consist of a large volume fraction of eutectic silicon. The morphology of eutectic Si is therefore of prim importance. This is due to its reported effects [1] on the final mechanical properties of the alloy. In commercial Al−Si alloys such as A356 or A360, the eutectic Si was described as coarse needle-like phase [1,2]. These coarse Si particles with their sharp ends promote stress concentrations and hence, they are detrimental to the mechanical properties as reported earlier [2,3]. In order to overcome this problem, several methods were proposed and applied to decreasing the size of these coarse particles and to rounding their sharp ends. Examples of these methods are: chemical modification via adding certain elements, quench modification by applying rapid cooling rate, processing in the semi-solid state, stirring using an electromagnetic field or ultrasonic vibrations [4−15]. Among the aforementioned modification methods [16−24], addition of elements to act as chemical modifiers is the most effective way to modify the eutectic Si. In this method, the morphology of Si phase is changed by minor addition of elements such as Na, Sr and Sb or by adding rare earth elements to the melt which effectively alter the sharp-ended Si phase to fibrous morphology and accordingly enhance the mechanical properties of the Al−Si alloys.

Different mechanisms were suggested to explain the eutectic modification by chemical modifiers. The most accepted mechanisms were those related to the twinning of {111} [25,26]. According to the theoretical calculations found in Refs. [25,26], the growth twin is formed at the interface (eutectic Si/modifier) when the ratio of atomic radius of the element relative to that of Si ($r_{modifier}/r_{Si}$) is about 1.646 [27]. Since the chemical modifiers like Na, Sr, Sb, Ba, Ca, Y, Yb and misch metals achieve this atomic radius ratio relative to Si, they can work perfectly as chemical modifiers [25−27]. Concerning the rare earth elements, Eu and Yb have the most optimum ratios of 1.70 and 1.66 respectively while

Corresponding author: S. EL-HADAD; E-mail: shimahassan@cmrdi.sci.eg
DOI: 10.1016/S1003-6326(19)65043-0

other rare-earth elements (RE) have ratios in the range of 1.48 (Lu) to 1.61 (La) [28].

The rare-earth elements are usually used as elemental modifiers for eutectic silicon in spite of the possible problems due to oxidation at high temperature during material processing. In order to avoid these common problems, modification of eutectic Si using RE compounds instead of RE elements was proposed in the current study. As RE compound, Y_2O_3 was incorporated during the melting of A356 alloy and its influence as a chemical modifier on eutectic Si was evaluated at different addition levels. The effect of the modified microstructures on the tensile properties of hypoeutectic A356 alloy was also investigated.

2 Experimental

2.1 Materials and processing

In the current experiments, commercial Al (99.98 wt.% purity), Si (99.9 wt.% purity) and commercial pure Mg (99.8 wt.% purity) were used as starting charging materials. Melting process was carried out in a 200 kW medium frequency induction furnace with graphite crucible. Charges of about 20 kg of A356 alloy with the composition of Al−7Si−0.35Mg−0.25Cu (in wt.%) were prepared as the base alloy for this investigation. After complete melting, a sample was taken from the melt and analyzed using an optical emission spectrometer (FOUNDRY-MASTER Pro, Germany). The chemical composition of the alloy is given in Table 1. Afterwards, the slag was removed to guarantee cleanliness of the produced casting. Then, a mechanical stirrer made of stainless steel was introduced into the molten alloy inside the crucible to create a vortex. The rotation speed was adjusted to 600 r/min and the stirring continued for 5 min. The immersion depth of the stirrer was maintained at 2/3 of the melt bottom. The RE compound (Y_2O_3) with the size of about 20 μm was added in amounts of 0, 0.3, 0.6, 1.0, 1.5, 2.0 and 2.5 in wt.%. In order to ensure the wettability with the molten alloy, the RE compound was added in the form of premixed powder of Al−30 wt.%Y_2O_3. At the end, the melt was poured at about 750 °C into a cylindrical sodium silicate−CO_2 sand mold of 100 mm in outer diameter and 42 mm in inner diameter and 250 mm in length. The reason for using a cylindrical sodium silicate CO_2 sand mold is to reduce the effect of cooling rate on the microstructures of the prepared alloys.

Table 1 Chemical composition of prepared A356 alloy (wt.%)

Si	Mg	Cu	Fe	Al
7.36	0.23	0.103	0.107	Bal.

2.2 Materials characterization

The samples for metallography were cut at a position of 20 mm from the bottom of the cast samples, mechanically ground using SiC abrasive paper, and polished via standard routines. These samples were etched with a solution of 0.5 vol.% concentrated HF in 99.5 vol.% H_2O to reveal their microstructure. The microstructure and phase analysis were investigated by optical microscopy (OM) (model ZEISS, Germany), scanning electron microscope (SEM) (Model JSM−5410, Japan) equipped with energy-dispersive spectrometer (EDS) (model INCA PENTAFET X3, England). Three parameters (average length, average area and aspect ratio) of eutectic Si particles of investigated alloys were quantified by the digital image analyzer system (AxioVision SE64 Rel. 4.9). Thermal analysis using differential scanning calorimetry (DSC) (STA 409 CD, Germany) was carried out at a heating and cooling rate of 10 °C/min to investigate the eutectic temperature depression of the prepared A356 alloy due to the addition of Y_2O_3.

Tensile tests were performed using computer controlled and digital display electromechanical universal testing machine (model LFM−L−20KN (bench top), Switzerland) with a stretching rate of 0.1 mm/min. All tensile specimens were cut from the cast cylindrical bars at the same position and machined according to ASTM E8 standard. Moreover, the fracture surfaces were observed by SEM in order to evaluate the fracture mode.

3 Results and discussion

Figure 1 shows the optical micrographs (OM) of the as-cast A356 alloys without and with different amounts of Y_2O_3. Furthermore, the effects of Y_2O_3 additions on the average length, average area and aspect ratio of eutectic Si for the investigated A356 are shown in Figs. 2−4, respectively. The common feature of all alloys is the dendritic primary α(Al) phase, surrounded by Al−Si eutectic structures [29] which varies with the Y_2O_3 content. It is evident that adding Y_2O_3 to A356 alloy modified the eutectic Si, but it had no noticeable effect on the primary α(Al) phase. Without Y_2O_3 addition, the Si morphology is typically coarse and flaky (Fig. 1(a)) with average length of 44.8 μm (Fig. 2), average area of 20.4 μm^2 (Fig. 3) and aspect ratio of 6.8 (Fig. 4), and is usually observed in foundry alloys when no chemical modifiers are added or the cooling rate is slow [30].

The 0.3 wt.% Y_2O_3 addition does not modify the morphology but causes a slight eutectic Si refinement (Fig. 1(b)) with average length of 11 μm (Fig. 2), average area of 20.1 μm^2 (Fig. 3) and aspect ratio of 4.8 (Fig. 4). The eutectic Si is further refined with increasing Y_2O_3 content (Figs. 1(c–e)). Moreover, with

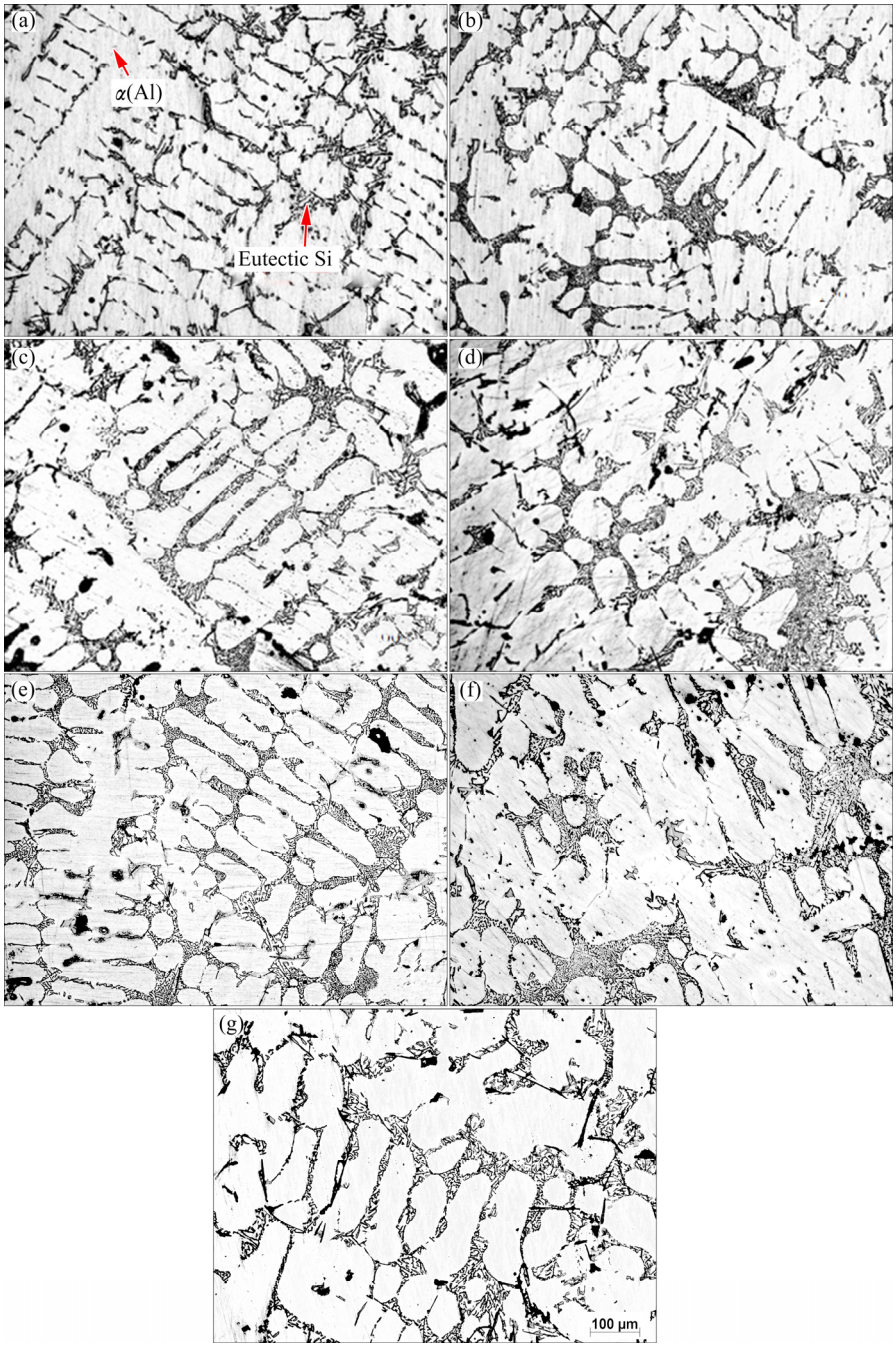

Fig. 1 Optical micrographs (OM) of as-cast A356 alloys without addition of Y_2O_3 (a) and with Y_2O_3 additions of 0.3 wt.% (b), 0.6 wt.% (c), 1 wt.% (d), 1.5 wt.% (e), 2 wt.% (f) and 2.5 wt.% (g)

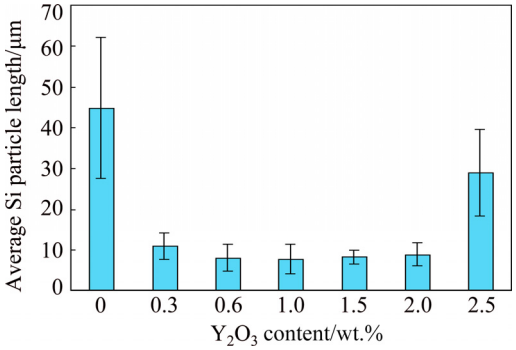

Fig. 2 Relationship between Y_2O_3 content and average length of eutectic Si

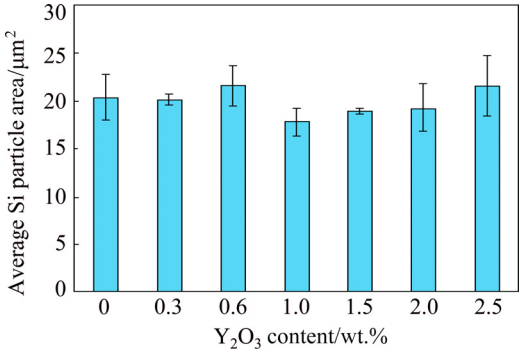

Fig. 3 Relationship between Y_2O_3 content and average area of eutectic Si

1.5 wt.% Y_2O_3, many fine fibrous and spherical morphologies of eutectic Si with average length of 8.3 μm (Fig. 2), average area of 18.9 μm^2 (Fig. 3) and aspect ratio of 0.98 (Fig. 4) are formed. However, the eutectic Si of needle and short rod abnormally appears when the addition of Y_2O_3 is increased to 2 wt.% and 2.5 wt.% (Figs. 1(f) and (g)) which means the appearance of over-modification. Therefore, the optimal modification effect is obtained when the Y_2O_3 content in the investigated A356 alloy is 1.5 wt.%.

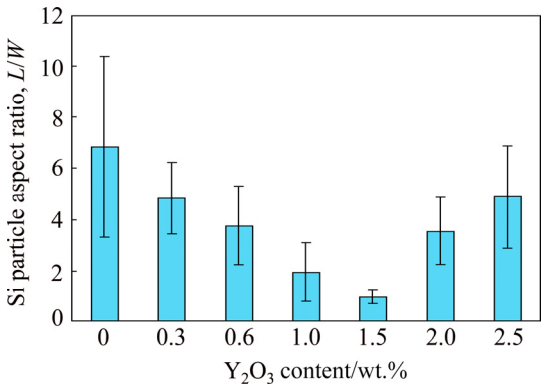

Fig. 4 Relationship between Y_2O_3 content and aspect ratio of eutectic Si

The typical SEM micrographs of the investigated A356 alloy without and with Y_2O_3 additions are illustrated in Fig. 5. It can be seen from Fig. 5(a) that coarse structures of flake-like, and long needle-like stick eutectic Si are formed. However, with 0.3 wt.%, 0.6 wt.% and 1 wt.% Y_2O_3 additions to the investigated A356 alloy, it is found that there are many short and fibrous structures of eutectic phase as shown in Figs. 5(b−d). With increasing Y_2O_3 addition up to 1.5 wt.% (Fig. 5(e)), it is observed that there are many fine spherical structures of eutectic phase. However, the eutectic Si of needle and short rod abnormally appears when the addition of Y_2O_3 is increased to 2 wt.% and 2.5 wt.% (Figs. 5(f) and (g)) which means the appearance of over-modification.

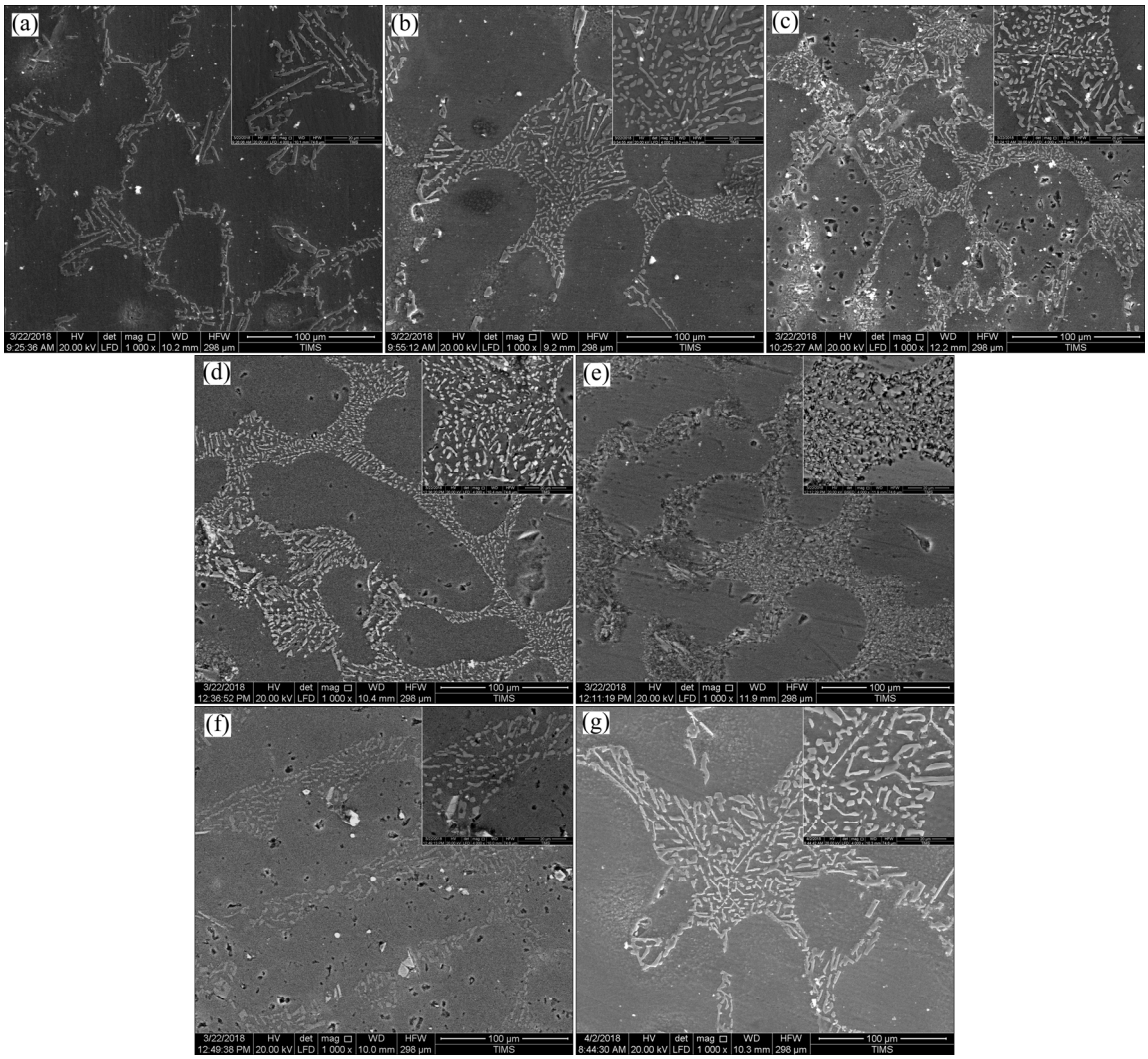

Fig. 5 SEM micrographs of investigated A356 alloy without Y_2O_3 addition (a) and with Y_2O_3 additions of 0.3 wt.% (b), 0.6 wt.% (c), 1 wt.% (d), 1.5 wt.% (e), 2 wt.% (f) and 2.5 wt.% (g)

The SEM micrograph of the investigated alloy with 1.5 wt.% Y_2O_3 addition is shown in Fig. 6(a) with EDS point analysis presented in Fig. 6(b). The elemental pattern shown in Fig. 6(b) demonstrates that the white particles contain Al, Y and Si. This implies that the intermetallic compound Al_3Y precipitates from the melt with the increasing of the addition amount of Y_2O_3 during the solidification. In Al−Y binary phase diagram [31], there is a eutectic reaction expressed as Eq. (1) [31] in the Al-rich corner of the diagram:

$$L \longrightarrow Al+Al_3Y \quad (1)$$

The temperature of the eutectic reaction is 637 °C, and the liquidus temperature of the A356 alloy is 615 °C; therefore, the eutectic reaction starts before the solidification of the liquid alloy. This eutectic reaction induced by RE leads to formation of the intermetallic compound Al_3Y. This compound is then segregated at the edge of eutectic Si and hence restricts the eutectic growth leading to modified eutectic Si in the investigated A356 alloy.

The scanning electron micrographs and the corresponding EDS elemental mapping of Al, Si, Y and O of the investigated A356 alloy with 1.5 wt.% and

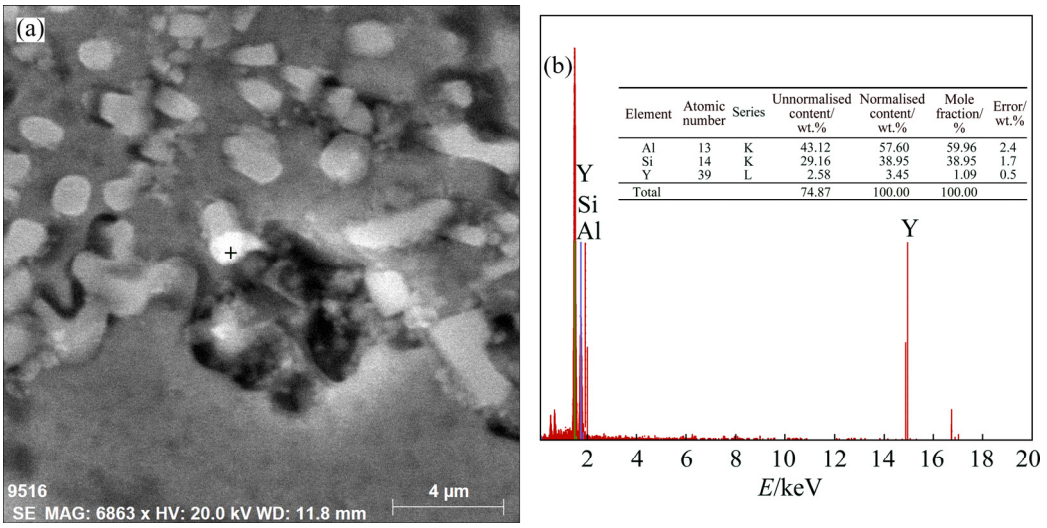

Element	Atomic number	Series	Unnormalised content/ wt.%	Normalised content/ wt.%	Mole fraction/ %	Error/ wt.%
Al	13	K	43.12	57.60	59.96	2.4
Si	14	K	29.16	38.95	38.95	1.7
Y	39	L	2.58	3.45	1.09	0.5
Total			74.87	100.00	100.00	

Fig. 6 SEM micrograph of investigated A356 alloy sample with 1.5 wt.% Y_2O_3 addition (a) and corresponding EDS pattern (b)

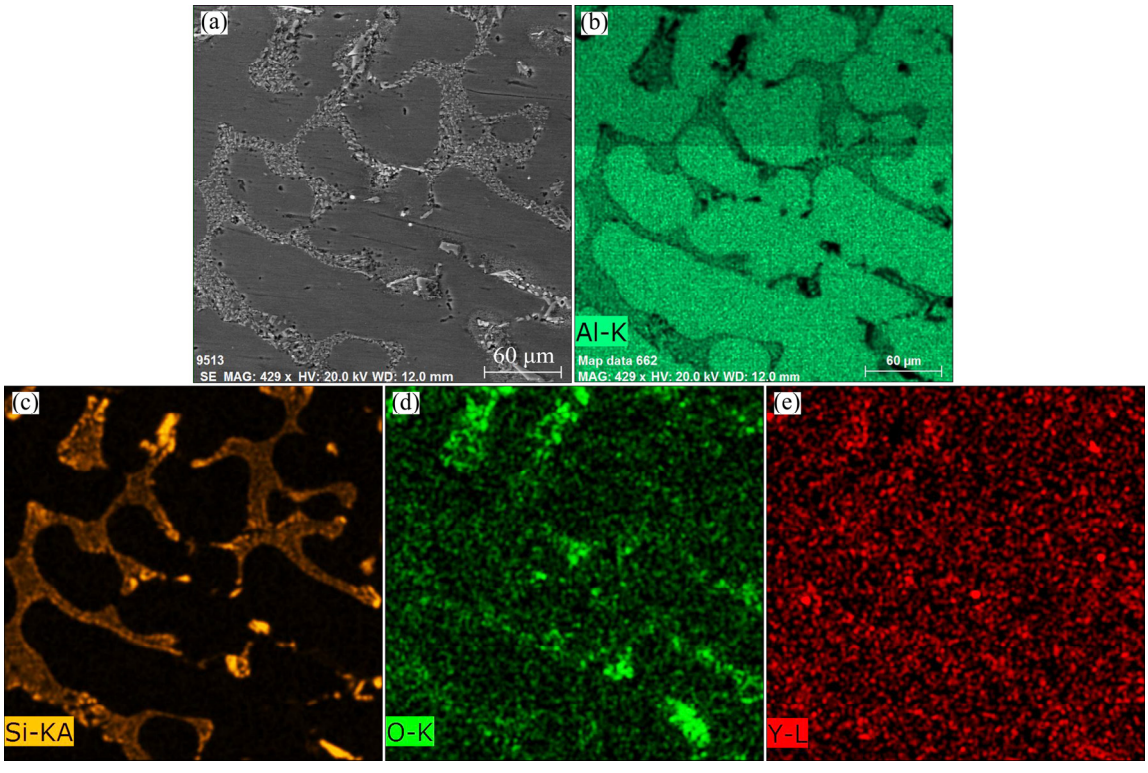

Fig. 7 SEM micrograph (a) and elemental mapping of Al (b), Si (c), O (d) and Y (e) of investigated A356 alloy with 1.5 wt.% Y_2O_3

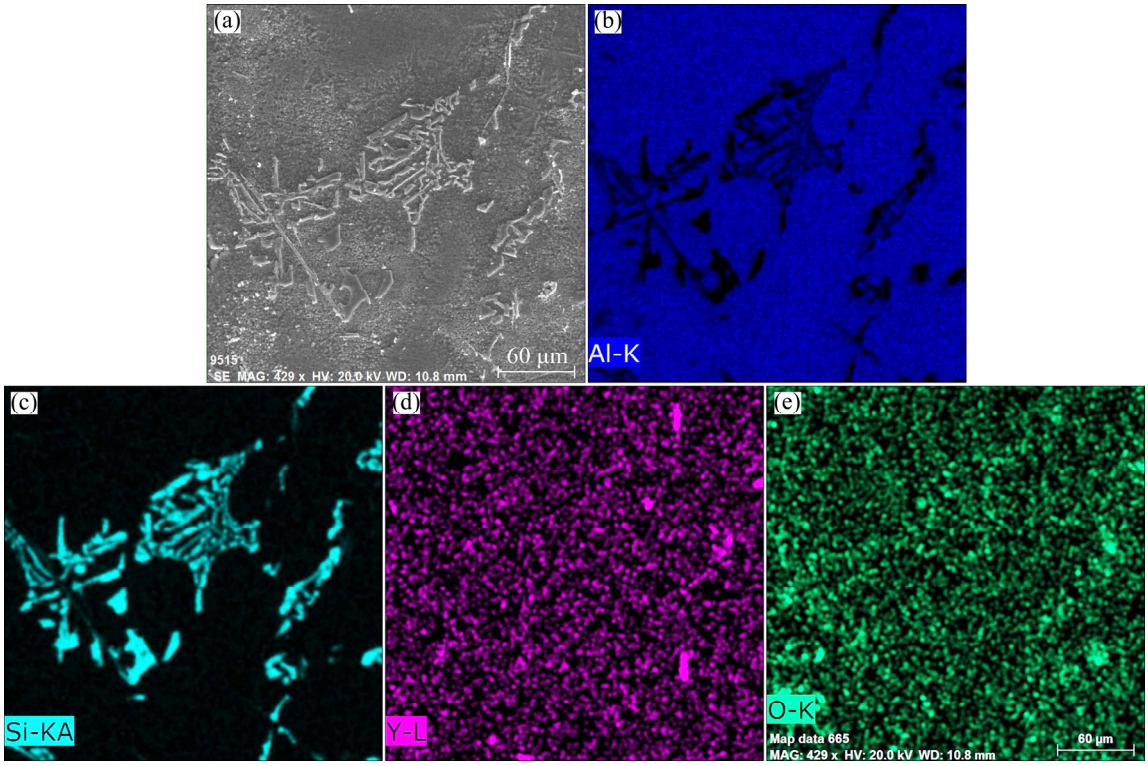

Fig. 8 SEM micrograph (a) and elemental mapping of Al (b), Si (c), Y (d) and O (e) of investigated A356 alloy with 2.5 wt.% Y_2O_3

2.5 wt.% Y_2O_3 are shown in Figs. 7 and 8, respectively. These EDS maps confirm the presence of α(Al) as a phase matrix and the eutectic silicon formed at grain boundaries. With 1.5 wt.% Y_2O_3 addition, the intermetallic compounds containing Y homogeneously distribute at the eutectic Si/Al interface and the edge of eutectic Si as shown in Fig. 7. On the other hand, agglomerates of the intermetallic compounds containing Y are frequently observed at the grain boundaries when Y_2O_3 addition increased to 2.5 wt.% as shown in Fig. 8. Combining Figs. 6 and 7, it is worth noting that O is rarely found associated with Y at the grain boundaries with 1.5 wt.% Y_2O_3 addition which is considered the optimum modification level. On the contrary, considerable amount of O is present at the grain boundaries in Fig. 8 where 2.5 wt.% Y_2O_3 was added and over-modification occurred. Here, the role of Y itself as RE modifier should be emphasized. Therefore, if Y is reduced from Y_2O_3, it can play the role of an effective modifier in the investigated A356 alloy. The possible reaction between Al and Y_2O_3 is expressed as Eq. (2):

$$2Al+Y_2O_3=Al_2O_3+2Y \quad (2)$$

According to the impurity induced twinning (IIT) theory [27], rare earth Y possesses effective modification ability for eutectic Si phase in the investigated A356 alloy because the atomic radius ratio of the modifying element Y (0.18 nm) to that of Si (0.117 nm) is 1.538 which is close to the ratio for twin growth (1.646) as reported earlier [32]. In fact, the eutectic Si phases produce lattice distortion when Y atom embeds into the lattice of Si due to the larger atomic volume of Y, which enhances the potential energy of the systems. A large number of twins are expected in the investigated A356 alloy which causes release of excess energy and hence helps to modify the Si phases. Therefore, the regular and fine fibrous eutectic Si can be obtained with the increase of rare earth Y concentration. However, further increase in the addition level of Y_2O_3 causes non-homogeneously distributed agglomerates at the grain boundaries thus leads to the over-modification shown in Fig. 8.

To further investigate the reason of modification of the eutectic Si crystals with Y_2O_3 addition, the eutectic temperature depression of each modified alloy was measured. Eutectic temperature depression is a general phenomenon associated with the modification of eutectic Si crystals [33]. Figures 9 and 10 show the DSC traces for A356 alloy without and with 1.5 wt.% and 2.5 wt.% Y_2O_3 additions during heating and solidification processes, respectively.

From these figures, it can be seen that the DSC curves of alloy with 1.5 wt.% and 2.5 wt.% Y_2O_3 shift left compared to that of Y_2O_3-free alloy, namely, the eutectic temperature is decreased with Y_2O_3 addition. Furthermore, the eutectic temperature with 1.5 wt.% Y_2O_3 is lower than that with 2.5 wt.% Y_2O_3 as indicated

in Figs. 9 and 10. Table 2 shows the peak eutectic temperature depression of each modified alloy during heating and solidification processes. Based on Table 2, Y_2O_3 addition can lower the crystallization temperature of the eutectic reaction, and the peak eutectic temperature depression with 1.5 wt.% Y_2O_3 is 4 °C during heating process and 11 °C during solidification process.

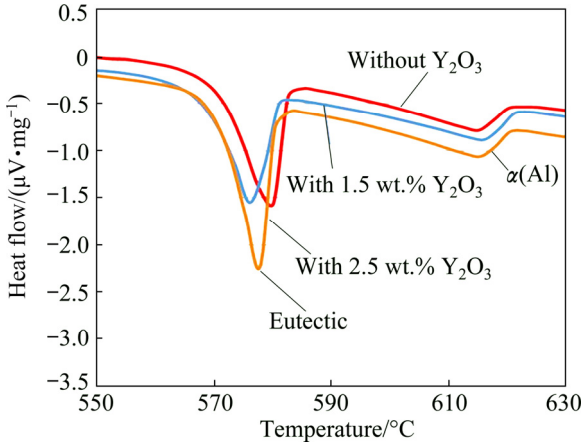

Fig. 9 DSC traces during heating process for investigated A356 alloy without and with Y_2O_3

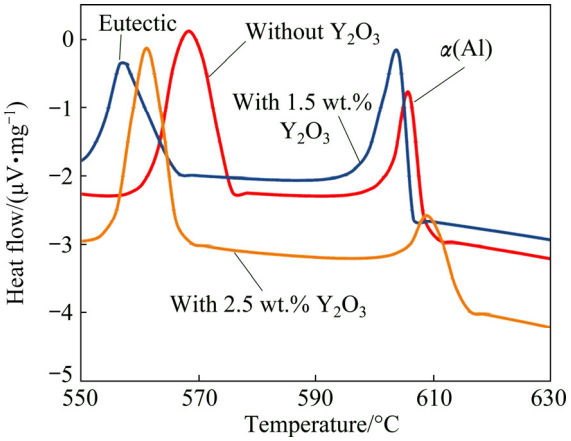

Fig. 10 DSC traces during solidification process for investigated A356 alloy without and with Y_2O_3

Table 2 Peak eutectic temperature depression of A356 alloy with Y_2O_3

Investigated alloy	Eutectic peak temperature/°C		Eutectic peak temperature depression/°C	
	Heating process	Solidification process	Heating process	Solidification process
A356	580	568	–	–
A356–1.5 wt.% Y_2O_3	576	557	4	11
A356–2.5 wt.% Y_2O_3	577.8	561	2.2	7

In other words, the eutectic-phase crystallization takes place under proper undercooling, and the increased undercooling is considered to be the result of modification. This is well consistent with the findings by NOGITA and DAHLE [34] and DAHLE et al [35]. They investigated the solidification mode of the eutectic phase in cast Al−7Si alloys by electron back-scattering diffraction and found that the eutectic nucleation mode is strongly dependent on the additive elements. It is suggested that the eutectic Si phases are modified as a result of the activation of some other nucleation sites for the eutectic cells under a certain undercooling. So, the eutectic temperature depression for modified alloy is approximately the same as the undercooling levels.

Figure 11 shows the results of ultimate tensile strength (UTS) and elongation (El) of the samples with different Y_2O_3 contents. It is obviously observed that UTS of the Y_2O_3-free alloy and Y_2O_3-containing alloys (0.3 wt.% and 1.5 wt.%) is practically the same. However, the alloys with (0.6 wt.%, 1 wt.%, 2 wt.% and 2.5 wt.%) Y_2O_3 exhibited lower UTS when compared to the Y_2O_3-free alloy. This reduction in strength may be attributed to the increase of porosity level in the composite in comparison with the matrix alloy. It was reported that there are several sources of gases in the casting process of the metal matrix composites [36,37]. The occurrence of porosity can be attributed to the amount of hydrogen present in the melt. This hydrogen can be drawn into the melt along with the surface oxide layer during the stirring process, especially in the case of vigorous stirring where the gas can be easily drawn and entrapped into the melt. In regard to the effect of modification on the ductility of A356 alloy, it is observed that the elongation distinctly improves with the increase of Y_2O_3 content up to 1.5 wt.% by 22.2% from 4.5% to 5.5% as shown in Fig. 11. This enhancement of elongation is due to the refinement and modification of

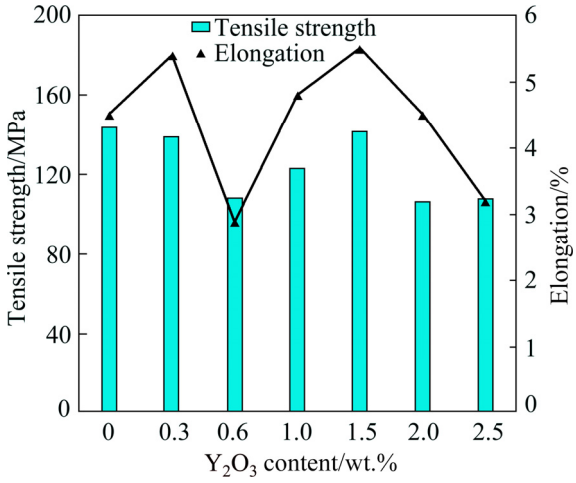

Fig. 11 Ultimate tensile strength and elongation of investigated A356 alloy with different contents of Y_2O_3

eutectic Si. However, the elongation decreases to 3.5% with increasing the addition of Y_2O_3 up to 2.5 wt.%. This reduction in elongation is attributed to the over modification which caused agglomeration of the intermetallic compounds containing Y at the grain boundaries as previously explained (Fig. 8).

Figure 12 presents the tensile fracture morphologies of A356 alloy without Y_2O_3 and with Y_2O_3 additions of 1.5 wt.% and 2.5 wt.%. In the Y_2O_3-free condition, the fracture surface is mainly covered by cleavage plane and local radial river patterns, as shown in Fig. 12(a). This indicates that the fracture mode is classical brittle fracture owing to the coarse structures of flake-like, and long needle-like eutectic Si distribution which have sharp edges, act as stress risers, which leads to a lower ductility [38]. On the other hand, Fig. 12(b) shows the fracture image of the A356 alloy with the addition of 1.5 wt.% Y_2O_3. It can be observed that some dimples form on the fracture surface, which demonstrates that the fracture mode of A356 alloy gradually transforms into ductile and brittle mixed fracture mode, which can be owed to the refinement and modification of eutectic Si [39]. However, the elongation reduces when the content of Y_2O_3 is 2.5 wt.% (Fig. 12(c)). This may be because the stiff and brittle rare earth compounds weaken the ability of plastic deformation of A356 alloy. The results of tensile properties and fracture surface illustrate that the unmodified A356 alloy belongs to the brittle failure type and the modified A356 alloy with 1.5 wt.% Y_2O_3 presents the ductile-brittle fracture mode. According to the explanation proposed here, it appears that characteristics of the intergranular eutectic modification among the large primary α(Al) grains control the elongation behavior of the experimental alloy rather than the primary α(Al) grains.

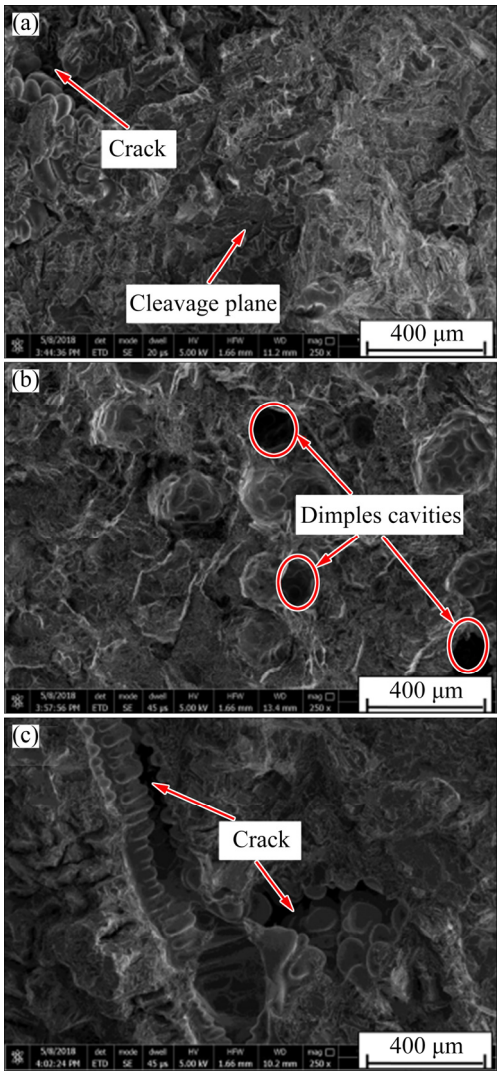

Fig. 12 Tensile fracture morphologies of investigated A356 alloy without Y_2O_3 (a) and with Y_2O_3 additions of 1.5 wt.% (b) and 2.5 wt.% (c)

4 Conclusions

(1) The optimum addition level was found to be 1.5 wt.% Y_2O_3, where the eutectic temperature of A356 alloy was reduced from 568 to 557 °C. Further addition up to 2.5 wt.% raised the eutectic temperature to 561 °C, indicating the loss of modification.

(2) Using the optimum addition level, the average Si particle length was decreased from 44.8 to 8.3 μm, the average area from 20.4 down to 18.9 μm^2 and accordingly the average aspect ratio was reduced from 6.8 to 0.98.

(3) The ductility of A356 alloy significantly increased by 22.2% from 4.5% to 5.5% at the optimum addition amount (1.5 wt.%) without reduction of tensile strength.

(4) With the refinement and modification of eutectic Si structure, the fracture mode gradually transfers from classic cleavage transgranular fracture to the ductile-brittle fracture mode.

Acknowledgements

The authors would like to appreciate the financial support from the Central Metallurgical Research and Development Institute (CMRDI), Ministry of Scientific Research, Egypt.

References

[1] LUDWIG T H, SCHONHOVD D E, SCHAFFER P L, ARNBERG L. The effect of Ca and P interaction on the Al–Si eutectic in a hypoeutectic Al−Si alloy [J]. Journal of Alloys and Compounds, 2014, 586: 180−190.

[2] CHEN Zhong-wei, MA Cui-ying, CHEN Pei. Eutectic modification of A356 alloy with Li addition through DSC and Miedema model [J]. Transactions of Nonferrous Metals Society of China, 2012, 22: 42−46.

[3] VANDERSLUIS E, SEDIAKO D, RAVINDRAN C, ELSAYED A, BYCZYNSKI G. Analysis of eutectic silicon modification during

solidification of Al−6Si using in-situ neutron diffraction[J]. Journal of Alloys and Compounds, 2018, 736: 172−180.

[4] LIU W Y, XIAO W L, XU C, LIU M W, MA C L. Synergistic effects of Gd and Zr on grain refinement and eutectic Si modification of Al−Si cast alloy [J]. Materials Science and Engineering A, 2017, 693: 93−100.

[5] WU Y P, WANG S J, LI H, LIU X F. A new technique to modify hypereutectic Al−24%Si alloys by a Si−P master alloy [J]. Journal of Alloys and Compounds, 2009, 477: 139−144.

[6] ZHANG Yu, WANG Yu-xin, LIAO Wen-jun, WANG Hua-yu, YANG Ying, YAN Biao. Modification mechanism of RE on hypereutectic AlSi alloy [J]. Metallic Functional Materials, 2010, 17: 86−90.

[7] KNUUTINEN A, NOGITA K, McDONALD S D, DAHLE A K. Modification of AlSi alloys with Ba, Ca, Y and Yb [J]. Journal of Light Metals, 2001, 1: 229−240.

[8] NOGITA K, YASUUDA H, YOSHIYA M, McDONALD S D, UESUGI K, TAKEUCHI A, SUZUKI Y. The role of trace element segregation in the eutectic modification of hypoeutectic AlSi alloys [J]. Journal of Alloys and Compounds, 2010, 489: 415−420.

[9] TSAI Y C, CHOU C Y, LEE S L, LIN C K, LIN JC, LIM S W. Effect of trace La addition on the microstructures and mechanical properties of A356 (Al7Si0.35Mg) aluminum alloys [J]. Journal of Alloys and Compounds, 2009, 487: 157−162.

[10] ROEHLING J D, COUGHLIN D R, GIBBS J W, BALDWIN J K, MERTENS J C E, CAMPBELL G H, CLARKE A J, MCKEOWN J T. Rapid solidification growth mode transitions in Al−Si alloys by dynamic transmission electron microscopy [J]. Acta Materialia, 2017, 131: 22−30.

[11] JUNG J G, LEE S H, CHO Y H, YOON W H, AHN T Y, AHN Y S, JUNG M L. Effect of transition elements on the microstructure and tensile properties of Al−12Si alloy cast under ultrasonic melt treatment [J]. Journal of Alloys and Compounds, 2017, 712: 277−287.

[12] JIAN X, XU H, MEEK T, HAN Q. Refinement of eutectic silicon phase of aluminum A356 alloy using high-intensity ultrasonic vibration [J]. Scripta Materialia, 2006, 54: 893−896.

[13] KHALIFA W, EL-HADAD S, TSUNEKAWA Y. Microstructure evolution and mechanical properties of sonoprocessed-thixocast AC4C billets [C]//Proc. 71st World Foundry Congress on Advanced Sustainable Foundry. Bilbao, Spain: Word Foundry Organization, 2014, 110056.

[14] KHALIFA W, EL-HADAD S, TSUNEKAWA Y. Microstructure characteristics and tensile property of ultrasonic treated-thixocast A356 alloy [J]. Transactions of Nonferrous Metals Society of China, 2015, 25: 3173−3180.

[15] KOTADIA H R, DAS A. Modification of solidification microstructure in hypo- and hyper-eutectic Al−Si alloys under high-intensity ultrasonic irradiation [J]. Journal of Alloys and Compounds, 2015, 620: 1−4.

[16] LI Q L, XIA T D, LAN Y F, ZHAO W J, FAN L, LI P F. Effect of rare earth cerium addition on the microstructure and tensile properties of hypereutectic Al−20%Si alloy [J]. Journal of Alloys and Compounds, 2013, 562: 25−32.

[17] CARDINALE A M, MACCIO D, LUCIANO G, CANEPA E, TRAVERSO P. Thermal and corrosion behavior of as cast Al−Si alloys with rare earth elements [J]. Journal of Alloys and Compounds, 2017, 695: 2180−2189.

[18] MAO F, YAN G Y, LI J Q, WANG T M, CAO Z Q. The interaction between Eu and P in high purity Al−7Si alloys [J]. Materials Characterization, 2016, 120: 129−142.

[19] TANG P, LI W F, ZHAO Y J, WANG K, LI W Z, ZHAN F. Influence of strontium and lanthanum simultaneous addition on microstructure and mechanical properties of the secondary Al−Si−Cu−Fe alloy [J]. Journal of Rare Earths, 2017, 35: 485−493.

[20] AHMAD R, ASMAEL M B A. Influence of lanthanum on solidification, microstructure, and mechanical properties of eutectic Al−Si piston alloy [J]. Journal of Materials Engineering and Performance, 2016, 25: 2799−2813.

[21] AHMAD R, ASMAEL M B A. Influence of cerium on microstructure and solidification of eutectic Al−Si piston alloy [J]. Materials Manufacturing and Processing, 2016, 31: 1948−1957.

[22] XU C, WANG F, MUDASSAR H, WANG C, HANADA S, XIAO WL, MA C. Effect of Sc and Sr on the eutectic Si morphology and tensile properties of Al−Si−Mg alloy [J]. Journal of Materials Engineering and Performance, 2017, 26: 1605−1613.

[23] YAN H, CHEN F H, LI Z H. Microstructure and mechanical properties of $AlSi_{10}Cu_3$ alloy with (La+Yb) addition processed by heat treatment [J]. Journal of Rare Earths, 2017, 34: 938−944.

[24] TIMPEL M, WANDERKA N, SCHLESIGER R, YAMAMOTO T, LAZAREV N, ISHEIM D, SCHMITZ G, MATSUMURA S, BANHART J. The role of strontium in modifying aluminum−silicon alloys [J]. Acta Materialia, 2012, 60: 3920−3928.

[25] HAMILTON D R, SEIDENSTICKER R G. Propagation mechanism of germanium dendrites [J]. Journal of Applied Physics, 1960, 31: 1165−1168.

[26] KOBAYASHI K F, HOGAN L M. The crystal growth of silicon in Al−Si alloys [J]. Journal of Materials Science, 1985, 20: 1961−1975.

[27] LU S Z, HELLAWELL A. The mechanism of silicon modification in aluminum–silicon alloys: Impurity induced twinning [J]. Metallurgical and Materials Transactions, 1987, 18: 1721−1733.

[28] NOGITA K, MCDONALD S D, DAHLE A K. Eutectic Modification of Al−Si alloys with rare earth metals [J]. Materials Transactions, 2004, 45: 323−326.

[29] HEGDE S, PRABHU K N. Modification of eutectic silicon in Al−Si alloys [J]. Journal of Materials Science, 2008, 43: 3009−3027.

[30] SHANKAR S, RIDDLE Y W, MAKHLOUF M M. Nucleation mechanism of the eutectic phases in aluminum–silicon hypoeutectic alloys [J]. Acta Materialia, 2004, 52: 4447−4460.

[31] LIU Zheng, LIU Xiao-mei, HU Yong-mei. Microstructure refinement by Y_2O_3 in semisolid A356 alloy [J]. Advanced Materials Research, 2011, 311−313: 666−669.

[32] QINGLIN L, BINQIANG L, JINBAO L, YUQIAN Z, TIANDONG X, Effect of yttrium addition on the microstructures and mechanical properties of hypereutectic Al−20Si alloy [J]. Materials Science and Engineering A, 2018, 722: 47−57.

[33] KANG H S, YOON W Y, KIM K H, KIM M H, YOON Y P, CHO I S. Effective parameter for the selection of modifying agent for Al−Si alloy [J]. Materials Science and Engineering A, 2007, 449−451: 334−337.

[34] NOGITA K, DAHLE A K. Effects of boron on eutectic modification of hypoeutectic Al−Si alloys [J]. Scripta Materialia, 2003, 48: 307−313.

[35] DAHLE A K, TAYLOR J A, GRAHAM D. The role of eutectic growth mode in porosity formation in Al−Si alloys [J]. Aluminum Transactions, 2000, 31: 17−30.

[36] LUSTER J W, THUMANN M, BAUMANN R. Mechanical properties of aluminum alloy 6061-Al_2O_3 composites [J]. Materials Science and Technology, 1993, 9: 853−862.

[37] TEKMEN C, OZDEMIR I, CONCEN U, ONEL K, The mechanical response of Al−Si−Mg/SiC_p composite: Influence of porosity [J]. Materials Science and Engineering A , 2003, 360: 365−371.

[38] SHAHA S K, CZERWINSKI F, KASPRZAK W, FRIEDMAN J, CHEN D L. Microstructure and mechanical properties of Al−Si cast alloy with additions of Zr−V−Ti [J]. Materials and Design, 2015, 83: 801−812.

[39] AHMAD R, ASMAEL M B A, SHAHIZAN N R, GANDOUZ S. Reduction in secondary dendrite arm spacing in cast eutectic Al−Si piston alloys by cerium addition [J]. International Journal of Minerals Metallurgical Materials, 2017, 24: 91−101.

Y_2O_3 化学改性对 A356 合金共晶硅特性和拉伸性能的影响

M. E. MOUSSA[1], S. EL-HADAD[1], W. KHALIFA[2]

1. Department of Casting Technology Central Metallurgical Research and Development Institute (CMRDI), P. O. 87, Helwan, Egypt;
2. Department of Mining, Petroleum and Metallurgical Engineering, Faculty of Engineering, Cairo University, P. O. 12613, Giza, Egypt

摘　要：通过添加氧化钇(Y_2O_3)对 A356 铝硅合金进行改性，其添加量为 0~2.5%（质量分数）。采用涡流法将预混粉末(Al−30%Y_2O_3)加入到 750 °C 熔体中，然后将样品倒入砂模。结果显示，添加 Y_2O_3 改性效果显著，其最佳添加量为 1.5%，此时共晶温度从 568 °C 下降到 557 °C。共晶硅颗粒尺寸由原来的 44.8 μm 细化到 8.3 μm，长宽比从 6.8 减小为 0.98。较高含量的 Y_2O_3 对共晶硅颗粒无改性作用。与未改性试样相比，改性试样的延展性提高了 20%以上。这与断裂模式从解理断裂逐渐过渡到更具韧性的断裂模式有关。

关键词：亚共晶 Al−Si 合金；改性；氧化钇(Y_2O_3)；延展性；断裂模式

(Edited by Xiang-qun LI)